Combustion of Liquid Hydrocarbons in a High-Speed Airstream

RAYMOND B. EDELMAN,* STEPHEN SCHMOTOLOCHA,† AND SIMON SLUTSKY‡
General Applied Science Laboratories Inc., Westbury, New York

A theoretical formulation and experimental results of the high-speed mixing, ignition, and combustion characteristics of liquid fuels injected directly into a high-velocity airstream are presented. Experiments were performed in a direct connect constant area combustor supplied by a Mach 2 air stream at a static pressure level of 1 atmosphere and at total temperatures ranging from ambient (530°R) to approximately 3300°R. The fuel was liquid hexane and was injected laterally into the supersonic flow through piloted and nonpiloted injector configurations. It was found that autoignition and stable combustion occurs for air total temperatures above about 2600°R. Furthermore, the liquid fuel was effectively ignited and burned stably below this autoignition level by employing a small reacting pilot jet. Minimum pilot size and energy requirements were then established. It was found that the pilot mass flows needed for ignition and sustained combustion were small compared to the main fuel and air flow rates. Comparison with theory indicates combustion efficiencies up to 93% were obtained.

Nomenclature

c_d = discharge coefficient
$\bar{d}$ = number weighted drop diameter
d_e = equivalent orifice diameter = $(4\dot{M}_j/\pi v_j \rho_j)^{1/2} = d_o(C_d)^{1/2}$
d_o = orifice diameter
H = stagnation enthalpy
h = static enthalpy
$(H_p)_p$ = pilot total sensible enthalpy
J = diffusional mass flux
M = Mach number
$\dot{M}$ = mass flow rate, lb/sec
p = pressure
$\bar{q}$ = $\rho_j v_j^2/\rho_\infty v_\infty^2$
r_p = particle radius
Pr = gas phase turbulent Prandtl number
Sc = gas phase turbulent Schmidt number
T = temperature
u = axial component of velocity
$\mathbf{v}$ = velocity vector
V = relative velocity
v = radial component of velocity
$\dot{W}$ = production rate
x = streamwise coordinate
Y = mass fraction in gas phase
y = lateral or radial coordinate
β = global mass fraction
δ_j = $\epsilon_{Tj}/\epsilon_{Tg}$
δ_p = particle bulk density
$(\Delta H_r)_{fl}$ = heat of combustion
ϵ_D = eddy diffusivity
ϵ_T = eddy conductivity
ϵ_v = eddy viscosity
θ_j = $\epsilon_{Dj}/\epsilon_{Dg}$
μ = absolute laminar viscosity
μ_t = turbulent viscosity
ξ = $\dot{M}_p(H_p)_p/\dot{M}_{fl}(\Delta H_R)_{fl}$
ρ = density
σ = surface tension
σ_j = $\epsilon_{vj}/\epsilon_{vg}$
τ_b = jet break-up time
τ_{ID} = ignition delay time
φ_0 = liquid fuel-combustor air equivalence ratio
φ_p = pilot equivalence ratio
ω = frequency

Subscripts

a = air
b = base of injector
fl = primary fuel (liquid hexane)
g = gas
i = ith gas phase component
j = jth particulate class or liquid jet conditions
l = liquid
0 = initial conditions
p = particle or pilot
t = local total conditions or turbulent
w = wall
∞ = freestream flow conditions

Superscript

$(\tilde{\ })$ = time average mass weight mean variable

Presented at the AIAA 8th Aerospace Sciences Meeting, New York, January 19–21, 1970; submitted February 24, 1970; revision received October 15, 1970. This work is supported by the Air Force Office of Scientific Research under Contract F44620-69-C-0056 with technical monitoring by B. T. Wolfson.

* Manager, Thermochemistry and Viscous Flow. Member AIAA.
† Project Scientist. Member AIAA.
‡ Staff Scientist; also Professor at New York University, Department of Aeronautics and Astronautics. Member AIAA.

I. Introduction

THE full realization of the performance potential of high-speed aircraft has long been a matter of interest since the conception of manned and unmanned hypersonic flight of well over a decade ago.

Problems of structural integrity, heat-transfer loads, compression and chemical dissociation losses preclude subsonic combustion in air breathing propulsion systems with applications directed toward flight Mach numbers greater than 4–6. Above this flight Mach number range supersonic combustion eliminates many of these problems and the theoretical performance is higher than would be realized if subsonic combustion were used.

The principal obstacle, anticipated by early workers in the field of supersonic combustion, was the shortness of the residence time in the combustion section compared to the fuel-air mixing time and the mixture combustion time.

Until very recently, the principal interest expressed in studies of high-speed airbreathing combustion systems was connected with purely gas phase systems. This was initiated about a decade ago with studies of the combustion characteristics of hydrogen air mixtures at supersonic speeds.[1–3] It was found that the chemical reaction rate characteristics were

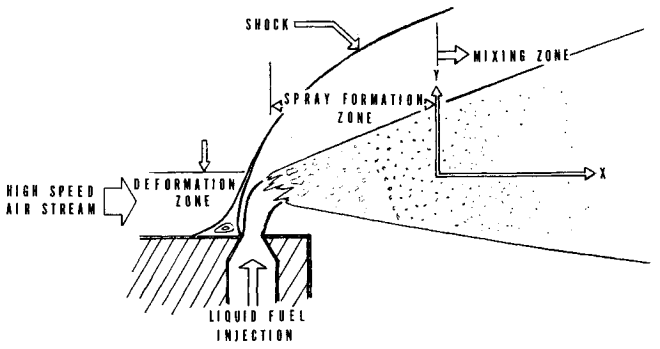

Fig. 1 Schematic of flowfield.

not necessarily the controlling parameters, but rather that the system that described the observed behavior was a basic coupling of chemical, heat conduction, molecular and free radical diffusion, and turbulent viscosity momentum transfer mechanisms.

The success with hydrogen was soon extended experimentally to combustion of the light gaseous hydrocarbons (methane, ethane, ethylene, propane) followed by a capability of representing hydrocarbon reactions through octane mathematically.[4,5] More recently further steps were taken with the extension of the problem to include the effects of multiphase mechanisms on the high-speed combustion process.

It is the purpose of this paper to describe the studies made to date upon the high-speed mixing and combustion characteristics of liquid fuels injected directly into a high-speed air stream.

II. Theoretical Considerations

The injection of a liquid into a flowing airstream can be described in terms of three physically distinct regimes. In the first, the liquid stream retains its identity and behaves as a deformable body undergoing distortions due to the complex interaction with the surrounding gas stream. The second regime involves the breakup of the distorted stream, ultimately yielding a cloud or spray of droplets with a size distribution depending upon the breakup mechanism. In the third and final regime the droplet cloud will undergo turbulent mixing with the surrounding gas stream. Depending upon the physical properties and states of the liquid and gas streams, evaporation and combustion can occur in all three flow regimes. Figure 1 shows a schematic of the flowfield with a delineation of the three zones of interest.

Liquid Stream Breakup

From elementary force balance considerations, it can be shown that the jet breakup time τ_b is approximately given by[6,7]

$$\tau_b = (d_o/v)(\rho_l/\rho_a)^{1/2} \tag{1}$$

where d_o is the jet diameter, v is the relative velocity component normal to the jet and ρ_l and ρ_a are the liquid and air stream densities, respectively.

During the time τ_b, the liquid stream is moving essentially across the high-speed air stream and at the same time is subjected to temperature and pressure levels appropriate to the normal shock values.

The effectiveness of this mechanism to reduce ignition times to an effective level depends upon the feasibility of attaining $\tau_b > \tau_{ID}$. The experimental program described in Sec. IV has provided data verifying this mechanism of ignition and demonstrates the applicability of the technique to practical systems.

Stable Droplet Size Distribution

To complete the description of the flow in the vicinity of the injection point the particle size distribution of the stable spray is required.

Adelberg[8] has considered liquid injection into a high-speed gas stream and the results of his analysis for the weighted drop diameter $\bar{d}$ is given by

$$\bar{d} = 65.3[\mu_l(\sigma_l/\rho_l)^{1/2}/\rho_a v^2]^{2/3} \tag{2}$$

where μ_l and σ_l are the viscosity and surface tension of the liquid, respectively. Although this representation is an idealization it provides a starting point for the spray mixing and combustion analysis. Ultimately the detailed size distribution will be required and additional experimental work in this area is needed.

Mixing Zone

In a practical flow configuration the spray will be formed in the very early part of the over-all domain of interest. Beyond the region dominated by the formation of the stable spray the flowfield will be controlled by the mixing and combustion processes. Although many studies have been made on multiphase flows few have dealt with suspensions of particulate matter in turbulent flow configurations of interest here.[9,12] The general problem involves the coupling of several mechanisms of mass, energy and momentum transport.[9] These include, turbulent dispersion, dynamic and thermal nonequilibrium between the phases, phase transition and homogeneous and heterogeneous chemical reactions. In the supersonic flow of current interest involving perpendicular injection of the liquid, particle sizes of the order of 5μ or less are easily obtainable. Thus, once the stable spray is formed it will be swept up to the air velocity in extremely short distances. In our experiments (Sec. IV), conservative estimates indicate velocity equilibration to within 1% occurs in the vicinity of the injector. This represents a fraction of the combustion chamber length and suggests two important features relevant to the analysis of the mixing and combustion zone. The first is that a condition of "near" dynamic equilibrium may be assumed. The second is that the flow geometry is amenable to a two-dimensional analysis initiating in the vicinity of the injector where the spray and air flows have become essentially parallel.

A third crucial element of the analysis involves the mechanisms of turbulent transport of the particulate cloud suspended in the gas stream. The problem is particularly complex owing to the lack of complete understanding of the turbulent structure in purely gas phase flows. Nevertheless, a small but finite body of literature does exist that provides some insight into the relationship between the parameters characterizing gas phase turbulence and those parameters characterizing the "response" of the particles. Perhaps the simplest functional relationship given is due to Longwell and Weiss[13]

$$\epsilon_{Dp}/\epsilon_{Dg} = [(\tfrac{9}{2})\mu_g/r_p^2\delta_p]\{\omega^2 + [(\tfrac{9}{2})\mu_g/r_p^2\delta_p]^2\}^{-1} \tag{3}$$

where ω is some "characteristic" frequency of the gas phase turbulence. Of course, there is no single frequency relevant to the transport process and one is hard pressed to compute such a characteristic frequency. Nevertheless, the dependence upon particle size is evident and "small" particles diffuse like a gaseous specie and "large" particles may not mix at all. In any given two phase flow, diffusive transport may be in equilibrium ($\epsilon_p = \epsilon_g$) or in general, nonequilibrium ($\epsilon_p \neq \epsilon_g$) with the "frozen" limit $\epsilon_p = 0$. The interested reader is referred to the more comprehensive discussion and review given by Soo.[14] For the present the relationships between particle and gas phase transport coefficients must be treated as parameters to be determined empirically.

The development of the describing equations for the steady turbulent flow of two phase systems in "near" dynamic equilibrium is detailed in Ref. 15. A key element of this analysis involves the definition of the turbulent fluxes and their relationship to the gradients of appropriate mean properties. The "near" equilibrium concept simply recognizes that an exact equality in velocities between the phases does not exist but that it is meaningful to characterize the global system with a single barycentric (mass mean) velocity in direct analogy with molecular diffusion. Furthermore, by applying Favre's[16] definition of mass weighted mean and fluctuating components of the instantaneous flow variables the confusion and controversy regarding recovery of the classical continuity equations for each phase and the appearance of second order correlations involving density fluctuations is eliminated. These definitions are given by

$$\rho = \langle\rho\rangle + \rho' \tag{4}$$

$$p = \langle p\rangle + p'' \tag{5}$$

$$u_\nabla = \tilde{u}_\nabla + u_\nabla'' \qquad \nabla = x,y,z \tag{6}$$

$$h = \tilde{h} + h'' \tag{7}$$

$$\beta_i = \tilde{\beta}_i + \beta_i'' \tag{8}$$

where

$$\langle Q''\rangle \neq 0, \quad \langle\rho Q''\rangle = 0, \quad \tilde{Q} = \langle\rho Q\rangle/\langle\rho\rangle; \tag{9}$$

$$Q = u_\nabla, \quad h, \quad \beta_i$$

Finally, the diffusivities of the particles will generally be different from those of the gas phase components precluding a straightforward application of Fick's Law to the global particle-gas system. A multicomponent diffusion law can be developed, however, by treating each particle class and the gas phase as a binary sub-system to which Fick's Law may be applied. The application of this notion gives the diffusional fluxes in the following form:

$$\mathbf{J}_{gi} = -\rho\epsilon_{Dg}\{\nabla\beta_{gi} - \beta_{gi}[(1 - \Sigma_j\theta_j\beta_{pj}/\beta_g)\nabla\beta_g + \Sigma_j\theta_j\nabla\beta_{pj}]\} \tag{10}$$

for the ith gas phase specie, and

$$\mathbf{J}_{pj} = -\rho\epsilon_{Dg}\theta_j\left\{\nabla\beta_{pj} - \beta_{pj}\left[\frac{1 - \Sigma_\mu(\theta_\mu\beta_{p\mu}/\theta_j)}{\beta_g}\nabla\beta_g + \Sigma_\mu\frac{\theta_\mu}{\theta_j}\nabla\beta_{p\mu}\right]\right\} \tag{11}$$

for the jth particle class, where

$$\rho\mathbf{v} = \rho_g\mathbf{v}_g + \Sigma_j\rho_{pj}\mathbf{v}_{pj} \tag{12}$$

$$\rho = \rho_g + \Sigma_j\rho_{pj} \tag{13}$$

and

$$\theta_j = \epsilon_{Dj}/\epsilon_{Dg} \tag{14}$$

$$\beta_g = \Sigma_i\beta_{gi} = 1 - \Sigma_j\beta_{pj} \tag{15}$$

The two limiting conditions defined by all $\theta_j = 1$ and all $\theta_j = 0$ are of interest for the small and large particle limits. For $\theta_j = 0$, for all j,

$$\mathbf{J}_{pj} = 0 \tag{16}$$

and

$$\mathbf{J}_{gi} = -\rho_g\epsilon_{Dg}\nabla Y_i \tag{17}$$

where Y_i is the ith gas phase specie mass fraction in the gas phase subsystem. For $\theta_j = 1$, for all j,

$$\mathbf{J}_{pj} = -\rho\epsilon_{Dg}\nabla\beta_{pj} \tag{18}$$

and

$$\mathbf{J}_{gi} = -\rho\epsilon_{Dg}\nabla\beta_{gi} \tag{19}$$

Equation (17) is the usual representation for diffusion in the gas phase. Equations (18) and (19) show that for diffusive equilibrium the particles behave as any other gas phase specie.

Incorporating these relationships in the conservation laws results in the following describing equations for the steady turbulent flow of a polydisperse system in plane two-dimensional or axisymmetric boundary-layer type flows.[15]

Global continuity

$$\partial y^N\rho u/\partial x + \partial y^N\rho v/\partial y = 0 \tag{20}$$

Species diffusion

ith gas phase specie

$$\rho u\frac{\partial\beta_{gi}}{\partial x} + \rho v\frac{\partial\beta_{gi}}{\partial y} = \frac{1}{y^N}\frac{\partial}{\partial y}\left\{y^N\rho\epsilon_{Dg}\left[\frac{\partial\beta_{gi}}{\partial y} - \beta_{gi}\times\left(\frac{1 - \Sigma_j\theta_j\beta_{pj}}{\beta_g}\frac{\partial\beta_g}{\partial y} + \Sigma_j\theta_j\frac{\partial\beta_{pj}}{\partial y}\right)\right]\right\} + \dot{w}_{gi}{}^c + \Sigma_j\dot{w}_{pij}{}^F \tag{21}$$

jth particle class

$$\rho u\frac{\partial\beta_{pj}}{\partial x} + \rho v\frac{\partial\beta_{pj}}{\partial y} = \frac{1}{y^N}\frac{\partial}{\partial y}\left\{y^N\rho\epsilon_{Dg}\theta_j\left[\frac{\partial\beta_{pj}}{\partial y} - \beta_{pj}\left(\frac{1 - \Sigma_\mu(\theta_\mu\beta_{p\mu}/\theta_j)}{\beta_g}\frac{\partial\beta_g}{\partial y} + \Sigma_\mu\frac{\theta_\mu}{\theta_j}\frac{\partial\beta_{p\mu}}{\partial y}\right)\right]\right\} + \dot{w}_{pj}{}^F \tag{22}$$

where for two-dimensional and axisymmetric flows $N = 0$ and 1, respectively; $\dot{w}_{gi} \equiv$ production of ith gas specie due to homogeneous gas phase reactions; $\dot{w}_{pij}{}^F \equiv$ production of ith gas phase specie from jth particle class due to evaporation or heterogeneous reactions; and $\dot{w}_{pj}{}^F \equiv$ production of the jth particle class.

Momentum

$$\rho u\partial u/\partial x + \rho v\partial u/\partial y = -dp/dx + (1/y^N)\partial/\partial y\{y^N\rho\epsilon_{vg}(\beta_g + \Sigma_j\sigma_j\beta_{pj})\partial u/\partial y\} \tag{23}$$

Energy

$$\rho u\frac{\partial H}{\partial x} + \rho v\frac{\partial H}{\partial y} = \frac{1}{y^N}\frac{\partial}{\partial y}\left(y^N\rho\epsilon_{vg}\left\{\frac{1}{Pr}\frac{\partial H}{\partial y} + \left[h_g\frac{1}{Sc}\Sigma_j\theta_j\beta_{pj} - \frac{H_g}{Pr} - \frac{1}{Pr}\left(\frac{Pr}{Sc} - 1\right)h_g - \frac{1}{Sc}\Sigma\theta_j h_{pj}\beta_{pj}\frac{1 - \Sigma_\mu(\theta_\mu/\theta_j)\beta_{p\mu}}{\beta_g}\right]\frac{\partial\beta_g}{\partial y} + \frac{1}{Pr}\Sigma\beta_{pj}(\delta_{pj} - 1)\frac{\partial H_{pj}}{\partial y} + \frac{1}{Pr}\left(\frac{Pr}{Sc} - 1\right)\Sigma_j h_{ig}\frac{\partial\beta_{gi}}{\partial y} + \Sigma_j\left[\theta_j\frac{(h_{pj} - h_g\beta_g)}{Sc} - \frac{H_{pj}}{Pr}\right]\frac{\partial\beta_{pj}}{\partial y} + \left[\beta_g\left(1 - \frac{1}{Pr}\right) - \Sigma_j\beta_{pj}\frac{\delta_j}{Pr}\right]\frac{\partial u^2/2}{\partial y} - \frac{1}{Sc}(\Sigma_j\beta_{pj}h_{pj})\left(\Sigma_\mu\theta_\mu\frac{\partial\beta_{p\mu}}{\partial y}\right)\right\}\right) \tag{24}$$

where

$$\theta_j = \epsilon_{Dj}/\epsilon_{Dg}, \quad \delta_j = \epsilon_{Tj}/\epsilon_{Tg}, \quad \sigma_j = \epsilon_{vj}/\epsilon_{vg}$$

and Pr, $Sc \equiv$ gas phase Prandtl and Schmidt numbers, respectively. The energy equation Eq. (24) may not, in general, be sufficient to define the thermal state of the system. Although dynamic equilibrium may be appropriate, the temperature of the particles can be sensibly different from the gas phase temperature depending upon the processes occurring on the particle scale. For evaporating droplets the local

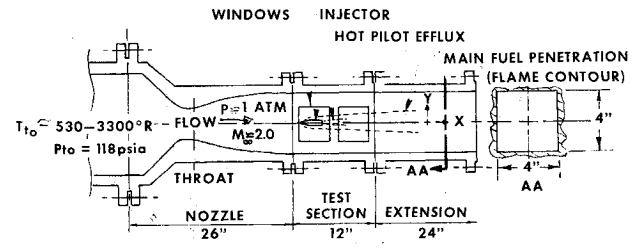

Fig. 2 Schematic of experimental apparatus for supersonic combustion of liquid injected hexane.

saturation temperature is appropriate. If metallic particles are involved and surface reactions are occurring then some other temperature is appropriate. Only in the case of inert particles (nonradiating) is there similarity in particle drag and heating processes for which "near" dynamic equilibrium would imply "near" thermal equilibrium. In cases where the thermal equilibrium assumption does not apply, Eq. (24) must be supplemented by either the gas-phase or particulate phase energy equation. The jth particulate phase energy equation is given by

$$\beta_{pj}\rho u\frac{\partial h_{pj}}{\partial x}+\beta_{pj}\rho v\frac{\partial h_{pj}}{\partial y}=q_{pj}+\frac{1}{y^N}\frac{\partial}{\partial y}\left(y^N\frac{\delta_{pj}}{Pr}\rho\epsilon_{v_g}\beta_{pj}\frac{\partial h_{pj}}{\partial y}\right)+\rho\epsilon_{D_g}\theta_j\left\{\frac{\partial\beta_{pj}}{\partial y}-\beta_{pj}\left[\frac{1-\Sigma_\mu(\theta_\mu\beta_{p\mu}/\theta_j)}{\beta_g}\right]\frac{\partial\beta_g}{\partial y}+\Sigma_\mu\frac{\theta_\mu}{\theta_j}\frac{\partial\beta_{p\mu}}{\partial y}\right\}\frac{\partial h_{pj}}{\partial y}\quad(25)$$

where q_{pj} is the heating rate of the interior of the jth particulate phase and h_{pj} is the static enthalpy of the particles.

Some observations on the above analysis should be noted. The particulate phase energy equations do not contain terms involving dissipation due to the "apparent" stress. The transport of momentum due to the random motion of the particles is a mechanical process affecting the particulate phase kinetic energy, but there is no mechanism by which this "apparent" shear can manifest itself directly as thermal energy of the particles.[15] Another interesting feature of the analysis is that it suggests an appropriate modification of the gas phase transport coefficients making it applicable to "near" dynamic equilibrium multiphase flows. For example Eq. (23) shows

$$\mu_t=[1+\Sigma_j(\sigma_j\beta_{pj}/\beta_g)]\mu_{tg}\quad(26)$$

where $\mu_{tg}=\rho_g\epsilon_{v_g}$ is the gas phase turbulent viscosity. Thus, assuming that the functional form of the gas phase transport coefficient is unchanged due to the presence of the particles one can apply an appropriate model for μ_{tg} and arrive at an effective global model for μ_t according to Eq. (26).

In the present problem, the empiricism involved in all three regimes of the liquid injection problem requires experimental data to validate and further develop the theoretical models. The following sections describe the current results of an experimental program which in addition to demonstrating the feasibility of high-speed combustion of liquids is providing data needed for the model development. Comparison of the above theory with experiments is given in Sec. V.

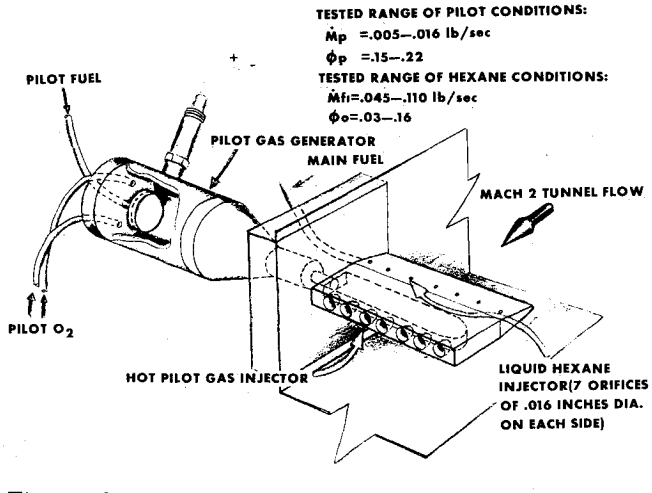

Fig. 3 Schematic of midstream piloted liquid hexane injector.

III. Experimental Study

Test Apparatus

The experiments were conducted in a Mach 2 combustion heated, blowdown wind tunnel over a total temperature range from ambient (530°R) up to 3300°R and a nominal stagnation pressure of 118 psia. The wind tunnel consisted of a vitiated heater, a two-dimensional nozzle with a 4-in. × 4-in. exit area, followed by a constant area combustor (test section) and optional combustor extension, as shown schematically in Fig. 2. Make-up oxygen was added to the vitiated air to maintain the correct mass fraction of atmospheric oxygen.

The primary fuel was normal hexane and was injected in the liquid phase at room temperature through the midstream strut injector configuration as shown in Figs. 2 and 3. Although this was the primary mode of injection, some tests were carried out with flush mounted injectors in the combustor top and bottom walls with fuel injected normal to the freestream.[6] It was found, however, that penetration, mixing, and combustion results were similar to those obtained with the midstream injection scheme. Hence, current emphasis was placed upon the midstream configuration because of symmetry wherein data could be more readily obtained and interpreted with the aid of analysis.

Injector Configuration

A schematic of the injector installed in the constant area combustor along with the range of test conditions are presented in Fig. 3. The configuration consists of three basic components: the liquid fuel injector, the pilot gas injector,

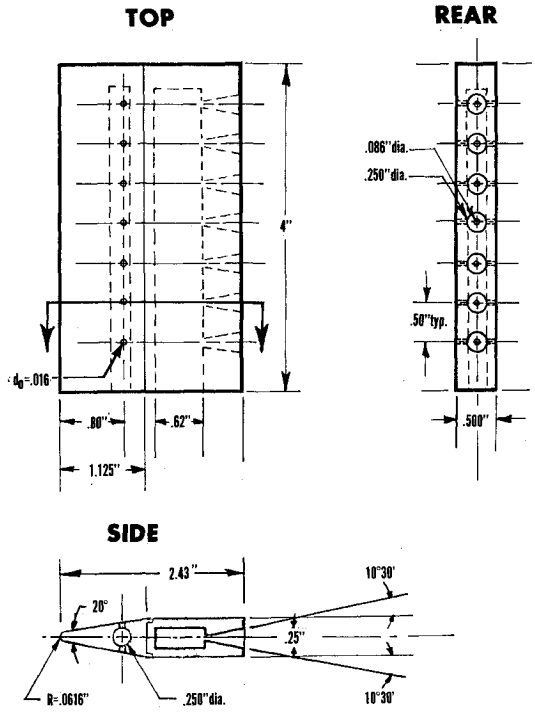

Fig. 4 Details of midstream piloted liquid fuel injector.

and the hot pilot gas generator. The first two were integrated and comprised the liquid fuel-gas pilot injector, details of which are shown in Fig. 4. This injector was then mounted across the midstream of the combustor. The pilot gas injector was designed and operated to yield matched pressures at the point of injection in the base region to minimize aerodynamic distortion.

The pilot gas generator was housed on the outside of the tunnel. It consists of a cylindrical combustion chamber, a mushroom type flameholder cooled by the pilot fuel, and an electrical spark source to initiate combustion. The pilot reactants were ethylene and oxygen. Once this mixture was ignited and steady pilot combustion was achieved the spark source was deactivated.

Piloting Technique

The concept behind this piloting technique is that it supplies a high-temperature gas core containing an abundance of free radicals. This hot gas core is generated by burning a small amount of fuel with an oxidizer in a lean proportion. The use of a lean mixture is selected for two reasons: first, it yields higher free radical concentrations than fuel rich mixtures, and second, the remaining free oxidizer is then available at elevated temperatures. Both the free radicals and high temperature combine to yield a very effective ignition source.

Instrumentation

Instrumentation included static pressure ports along top and bottom walls of the nozzle, test section, and extension duct; one-dimensional heat transfer gages mounted in the top wall from the base of the injector extending down to the exit plane of the extension; multiprobe Pitot rake, and a multiprobe fast response, fine wire shielded thermocouple rake to measure the freestream impact pressures and total temperatures, respectively. Tunnel stagnation conditions were monitored continuously as were the mass flows of the tunnel and test fluids.

In addition, still photography and cinematography combined with visual observations afforded the balance of the information acquired during the combustion and penetration tests.

IV. Experimental Results

Penetrations

The penetration tests were run with the bottom stainless steel combustor wall replaced by a plexi-glass wall to permit

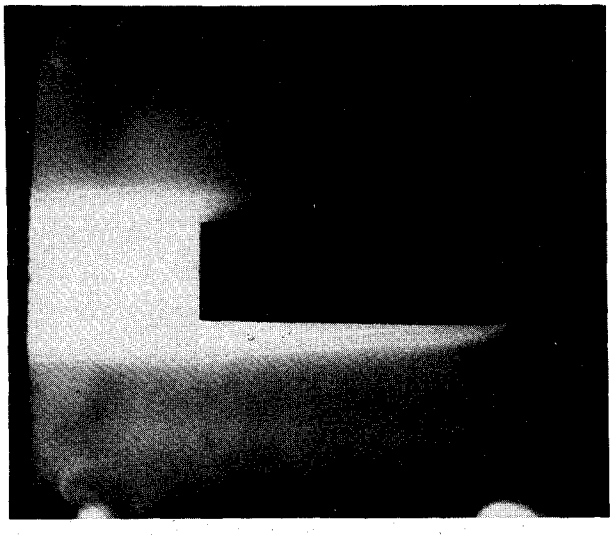

Fig. 5 Typical lateral injection of liquid hexane into a nonreacting $M_\infty = 2$ airstream at $T_{t_0} = 530°R$ and $P_{0j}/P_\infty = 37.2$, $\dot{M}_{fl} = 0.0745$ lb/sec.

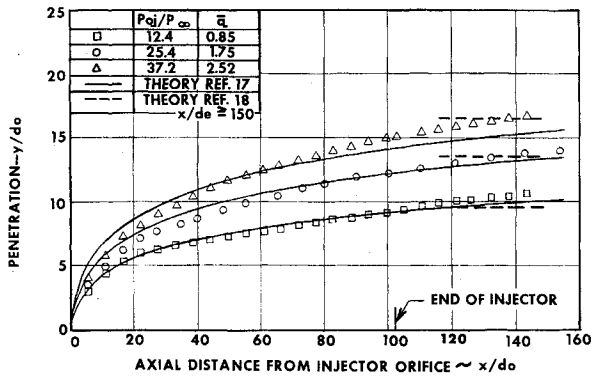

Fig. 6 Comparisons of jet penetrations of liquid hexane injected into Mach 2 airstream at $P_\infty = 1$ atm, $T_{t_0} = 530°R$, and $d_0 = 0.016$ in.

an electronic flash to illuminate the liquid jets from below. The photographs of the penetrations were taken through the windows provided on the side wall. These tests were carried out in nonreacting flows at air total temperature of 530°R. A typical photograph of the penetration of liquid hexane injected into a Mach 2 airstream is shown in Fig. 5.

The measurements of the x-y coordinates of the penetration trajectories were then obtained from enlarged photographs. Some of the results are presented in Fig. 6. In addition to supplementing existing data, the agreement validates the use of existing prediction techniques to aid in establishing the initial conditions required in the theoretical analysis for the primary mixing and combustion zone.

Autoignited Combustion

Several injectors were tried during the early phases of the high temperature autoignition tests. In all cases combustion was achieved with remarkably little difficulty. With air total temperature in the neighborhood of 3000°R very rapid combustion was always attained. In fact, heat-transfer rates in the neighborhood of the injector were so great that several injector rigs were burned out early in the program. A flush mounted wall injector and the midstream injector were tested extensively to determine the effects of air temperature φ_0 and injector geometry on ignition and combustion characteristics. It was found that autoignition followed by intense combustion could be obtained for air total temperatures as low as 2600°R. Also variation in φ_0 or the injector configuration had no effect either on ignition or this critical temperature level.

When the total temperature of the airstream was decreased below this value no flame generation was observed. However, an interesting phenomenon was observed from a photograph taken of the fuel injection region during a test at an air total temperature of about 2500°R. It showed an initial region of luminosity with a sharp front at the line of injection followed by rapid fading as the flow moved downstream, and finally disappearing in a distance of about $1\frac{1}{2}$ in. This observation is consistent with the mechanism discussed in Sec. II. Thus, it may be concluded that below the critical temperature the combustible mixture does not reside long enough within the region of high relative velocity and high static temperature and pressure to produce the conditions required for self-sustained combustion. The line of initial luminosity followed by fading is interpreted as ignition in the region of highest static temperature and pressure about the droplets followed by quenching as the droplets accelerate and the local temperature and pressure drop.

Autoignition at temperatures above this quenching limit is predicted by Eq. (1). Typically, $(d/v)(\rho_l/\rho_a)^{1/2} \equiv 70\mu$ sec whereas $\tau_{ID} \equiv 10\mu$ sec.

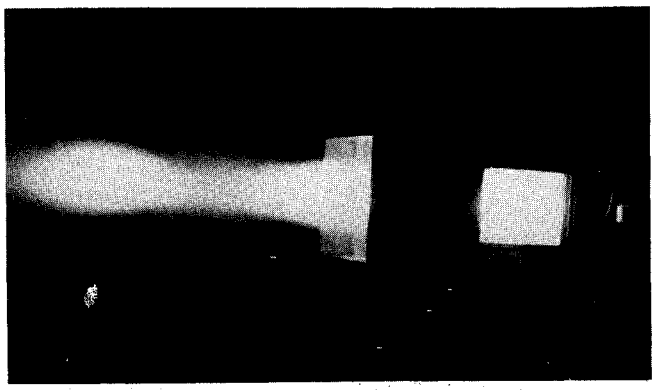

Fig. 7 Flame luminosity patterns of pilot ignited supersonic combustion at T_{t_0} = 1420°R, φ_0 = 0.076, $\dot{M}_p/\dot{M}_f$ = 0.244, and φ_p = 0.180.

Pilot Ignited Combustion

The objectives of the piloted mode of ignition were twofold. First, to obtain basic information on the characteristics of the pilot regarding the requirements to ignite and promote stable combustion of the liquid fuel for air temperatures below the 2600°R autoignition limit. Second, to assess the resulting mixing and combustion characteristics of the main fuel. The use of this pilot enabled combustion studies to be performed from the autoignition limit down to the ambient (530°R) air total temperature level.

A typical flame luminosity photograph is presented in Fig. 7. It corresponds to air total temperature of 1420°R, φ_0 = 0.076, a pilot to main fuel mass flow ratio of 0.244, and pilot equivalence ratio of 0.180. With the combustor extension duct removed, the visible luminous flame structure clearly indicates that combustion was supersonic. All supersonic combustion tests indicated similar flame contours and lengths. However, at 530°R air temperature where φ_0 = 0.036, $\dot{M}_p/\dot{M}_{fl}$ = 0.31 and φ_p = 0.181, the observed flame zones were reduced by as much as 80%. Although φ_0 in the low-temperature case was less than in the high-temperature cases, the reduction in flame length is associated with a substantially reduced combustion efficiency. It should be noted that these conditions would result in thermal choking if all the fuel were burned. However, the measured pressure distribution indicated that the flow was supersonic throughout the duct. Indeed, the comparison of the measured wall pressure with one-dimensional calculations indicated that only about 30% of the fuel was consumed. Nevertheless, this test revealed the ability of the pilot to ignite cold flows under supersonic conditions and it would be of interest to determine if the combustion efficiency could be substantially improved with a modest increase in pilot flow.

Finally, to evaluate the contribution of the pilot on the length and intensity of the flame zone, tests were run at identical conditions but without the main fuel flowing. Virtually, no luminosity was observed visually or photographically in the base of the injector.

V. Analysis of Combustion Results

Figure 8 shows axial wall pressure distributions for typical nonburning, autoignited combustion, pilot ignited combustion, and thermally choked pilot ignited combustion flows.

The nonburning tests are represented by a single curve and include the combined influence of the boundary-layer growth along the constant area duct, the presence (i.e., drag) of the injector with and without the main fuel injection, and with nonreacting and reacting pilot gases flowing. That these events are represented by a single curve is due to the fact that at the tested pilot and main fuel conditions, the flows associated with the pilot jet (i.e., hot or cold) as well as the main fuel (i.e., very lean fuel-air ratio) involved negligible momentum and energy addition to the main air flow. Hence, the "nonburning" curve establishes a base to compare with the effects of combustion.

The rise and fall of pressure (from station 26 to 30) is caused by the injector leading edge shock and the combined effects of shoulder plus the near base expansion waves, respectively. It is common to all burning and nonburning supersonic flows. However, the extent of the expansion depends upon the particular flow configuration as discussed previously.

Subsequently, the autoignited combustion flows shows a secondary pressure rise from station 30 in. to about 38 in. that reaches a peak value and then levels off. This suggests a strong pressure interaction mechanism between the region of intense heat release and the high-speed airstream. The combustion-induced pressure rise is thus quite rapid, but too smooth to be associated with the formation of a strong shock structure. This conclusion is substantiated by a comparison with the mixing analysis described in Sec. II. The calculation was carried out for a plane two-dimensional configuration assuming the combustion process was diffusion controlled. The initial conditions were based upon the state of flow in the plane of the injector base assuming that no significant reaction had yet taken place. The boundary conditions imposed on the constant area duct were zero heat and mass transfer. In addition, zero shear was assumed but the "tare" (nonburning) pressure rise was superimposed on the predicted pressure distribution. The result is shown in Fig. 8 and the agreement with the measurements is very good. This result is significant because it predicts the details of the process which cannot be obtained from a one-dimensional analysis. Furthermore, the comparison indicated that kinetics are not a controlling factor at these particular autoignition conditions and for comparative purposes a simple one-dimensional complete combustion calculation was carried out. This was done also neglecting the effects of pressure induced by the boundary layer growth along the duct and the injector drag. Then by superimposing the "tare" (nonburning) pressure rise upon the ideal combustion pressure rise, it was found to agree well (Fig. 8) with the actual downstream pressure and the diffusion controlled combustion prediction. In fact, this comparison indicates that a combustion efficiency of 90% was realized, where the combustion efficiency for lean mixtures is defined as the ratio of the theoretical equivalence ratio to the experimental equivalence ratio required to produce a given combustion pressure: $\eta_c = (\varphi_{0\ \text{theo}}/\varphi_{0\ \text{exp}})_{p_c}$, p_c = const. Now the pilot ignited combustion flow curve (c.f., Fig. 8) shows an earlier and more rapid pressure rise than the autoignited case. This indicates the effect of local intense heat release of the hexane-air mixture induced by the pilot in the vicinity of the base. Upon reaching a peak the pressure then

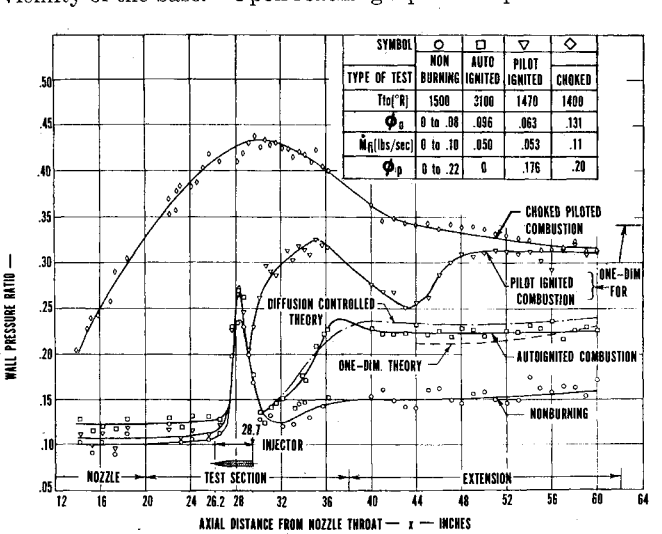

Fig. 8 Axial pressure rise induced by combustion of liquid injected hexane at $M_\infty \simeq 2$ and $P_\infty \simeq 1$ atm.

drops off. This drop is apparently caused by the diffusion of the pilot gases. However, self-propagation of the flame is then achieved and the pressure rises to a constant value downstream. As in the case of autoignited combustion, comparison of this "final" pressure level with a one-dimensional complete combustion model indicates again combustion efficiencies of 90% but at a slightly longer combustor length as depicted in Fig. 8. When the air total temperature was raised to 2000°R a combustion efficiency of 93% was achieved.

The extent of the axial pressure drop-off, from stations 35 to 43, caused by the diffusive dissipation of the pilot gases varied with the total initial air temperature. That is, the higher the air temperature, the smaller was the drop-off prior to self-propagation of the flame. In fact, for a given pilot condition there will exist an initial air temperature limit below which self-propagation of the flame can not be attained. Then the corresponding final pressure level will be somewhere between the pilot induced peak level and the nonburning level indicating incomplete combustion of the fuel. An example of this case is the aforementioned 530°R air total temperature test, during which self-propagation of the flame could not be maintained.

The uppermost curve in Fig. 8 represents a typical axial pressure distribution for a combustion induced choked flow. It shows very clearly, that for the indicated test conditions, a supersonic flow could not be maintained resulting in an altered flow in the diverging section of the nozzle. A one-dimensional complete combustion calculation for the fuel-air mixture at this test condition showed that thermal choking should have indeed occurred. In fact, for this test the calculations indicated that in order to burn the fuel supersonically φ_0 must be less than about 0.095.

Some total temperature profiles at two axial stations for nonburning and burning flows are shown in Fig. 9. The degree of nonuniformity at the initial station, 10 in. downstream from the injector base, compared with the profiles at 34 in. from the injector base indicate the combined effects of mixing and combustion and provide data of the type needed for comparison with the mixing and combustion analysis. The mean temperature level for this case at 34 in. was compared with simple one-dimensional complete combustion calculations and a value of $T_t/T_{t_0} = 1.23$ was obtained. This indicates that combustion was completed or nearly completed in about 2 ft of the chamber. In general, Pitot pressure measurements reflected consistent behavior with the total temperature profiles.

Minimum Pilot Requirements for Ignition

The results of the pilot ignited combustion tests have been further reduced into a composite curve defining combustion limits over the spectrum of air total temperatures. Presented in Fig. 10 are the minimum pilot requirements for

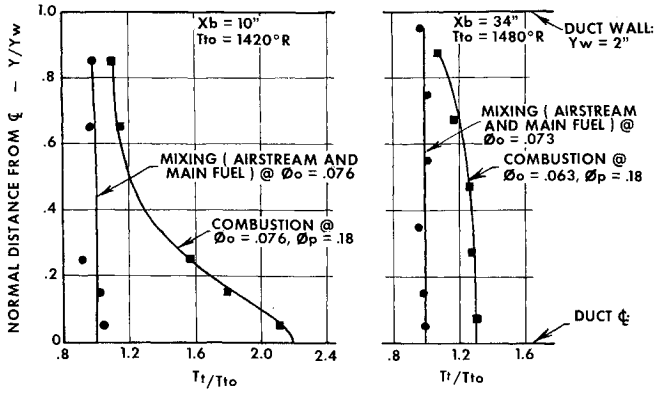

Fig. 9 Total temperature profiles of supersonic mixing and combustion (pilot induced) of liquid injected hexane at $M_\infty \simeq 2$ and $P_\infty \simeq 1$ atm.

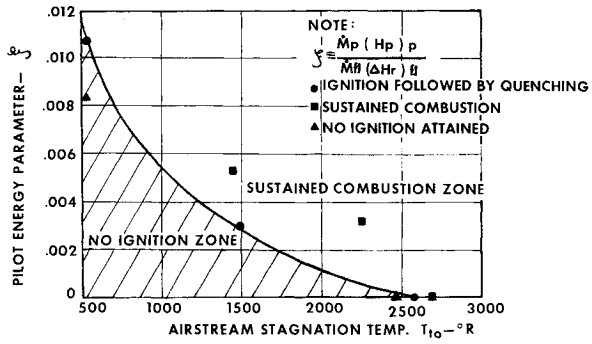

Fig. 10 Minimum mass flow requirements for ignition of injected liquid hexane $M_\infty \simeq 2$, $P_\infty \simeq 1$ atm and pilot $\varphi_p \approx 0.19$, $\dot{M}_p \approx 0.016$ lb/sec.

fixed pilot equivalence ratio expressed in terms of the ratio of total pilot mass flow to the main fuel mass flow as a function of the air total temperature.

Figure 11 demonstrates the same results but using an energy ratio, defined as pilot products sensible energy over the main fuel heat of combustion. It shows the small pilot energy requirements necessary to achieve supersonic combustion of the liquid fuel. The low-energy requirement is associated with the presence of highly reactive free radicals and consequently caution must be exercised when comparing this energy parameter with other ignition techniques. Since the presence of the free radicals is a natural consequence of the pilot gas generator technique it makes this method attractive for practical applications.

VI. Conclusions

The studies presented in this report have led to the following observations.

Conditions of spray formation, residence time and local thermodynamic state can be controlled to obtain ignition and combustion of liquid hydrocarbon fuels injected directly into a supersonic air stream. An analytical framework describing this type of polydisperse system has been developed. This includes the injection region and the downstream mixing and combustion zone. Reliable hexane autoignition was obtained for air flowing at Mach 2 with stagnation temperatures of 2600°R or more using both wall and midstream injectors following by very intense combustion heat release.

The controlling parameters in the ignition mechanism can be related to the acceleration wave mode of liquid stream breakup and the local air stream stagnation state. Thus the residence time for the autoignition experiments was typically $(d/v)(\rho_l/\rho_a)^{1/2} \cong 70\mu$ sec, whereas the ignition delay time based on the local stagnation conditions is $\tau_{ID} \cong 10\mu$ sec. Hence, autoignition is predicted and observed.

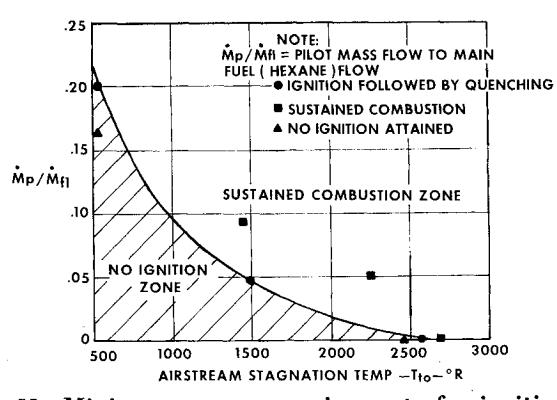

Fig. 11 Minimum energy requirements for ignition of injected liquid hexane $M_\infty = 2$, $P_\infty = 1$ atm and $\dot{M}_p = 0.005$–0.016 lb/sec, $\dot{M}_{fl} = 0.110$ lb/sec.

An appropriate piloting technique resulted in stable ignition and combustion for air temperatures ranging from 2600°R down to ambient (530°R). In addition, combustion efficiencies of over 90% were obtained over the bulk of the total temperature spectrum.

Minimum pilot requirements were established and show that ignition can be achieved with total pilot-to-main-fuel mass flow ratios of 20% or less. This is partially accounted for by the presence of highly reactive free radicals which makes the pilot gas generator technique of ignition most attractive for practical applications.

References

[1] Libby, P. A., Pergament, H. S., and Bloom, M. H., "A Theoretical Investigation of Hydrogen-Air Reactions. Part I—Behavior with Elaborate Chemistry," TR 250, Aug. 1961, General Applied Science Labs. Inc., Westbury, N. Y.

[2] Pergament, J. S., "A Theoretical Analysis of Non-Equilibrium Hydrogen-Air Reactions in Flow Systems," AIAA Paper 63-113, Washington, D.C., 1963.

[3] Westenberg, A. A., "Hydrogen-Air Chemical Kinetic Calculations in Supersonic Flow," CM-1028, Dec. 1962, Applied Physics Lab., Johns Hopkins Univ., Md.

[4] Chinitz, W. and Baurer, T., "An Analysis of Non-Equilibrium Hydrocarbon-Air Combustion," TR 546, Aug. 1965, General Applied Science Lab., Inc., Westbury, N. Y.; also presented at the Fall 1965 Meeting of the Western States Section, The Combustion Institute, Santa Barbara, Calif., Oct. 25–26, 1965.

[5] Edelman, R. and Fortune, O., "A Quasi-Global Chemical Kinetic Model for the Finite Combustion of Hydrocarbon Fuels with Application to Turbulent Burning and Mixing in Hypersonic Engines and Nozzles," AIAA Paper 69-86, New York, 1969.

[6] Slutsky, S., Williams, F., and Tamagno, J., "Ignition and Combustion of Liquid Hydrocarbon Fuels in Supersonic Flows," TR 724 AFOSR-69-1390, June 1969, General Applied Science Labs. Inc., Westbury, N. Y.

[7] Heidmann, M. F. and Groeneweg, J. F., "Analysis of the Dynamic Response of Liquid Jet Atomization to Acoustic Oscillations," TND 5339, July 1969, NASA.

[8] Adelberg, M., "Mean Drop Size Resulting from the Injection of a Liquid Jet into a High-Speed Gas Stream," *AIAA Journal*, Vol. 6, No. 6, June 1968, pp. 1143–1147.

[9] Edelman, R. and Rosenbaum, H., "Generalized Viscous Multicomponent-Multiphase Flow with Application to Laminar and Turbulent Jets of Hydrogen," AIAA Paper 63-507, Palm Beach Fla., 1963; also TR 349, June 1963, General Applied Science Labs., Westbury, N. Y.

[10] Smoot, L. D., Coates, R. L., and Simonsen, J. J., "Mixing and Combustion of Compressible Particle Laden Ducted Flows," AIAA Paper 69-460, U. S. Air Force Academy, Colo., 1969.

[11] Channapragada, R. S., Anderson, J., Turumalesa, D., and Gopalakrishnan, A., "Mixing, Igniton, and Combustion Analysis of Air-Augmented Solid Rockets with Boron Particles," *AIAA Journal*, Vol. 7, No. 8, Aug. 1969, pp. 1581–1587.

[12] Genevese, J., Edelman, R., and Fortune, O., "Some Aspects of Two Phase Flows with Mixing and Combustion in Bounded and Unbounded Flows," AIAA Paper 70-145, New York, 1970.

[13] Longwell, J. P. and Weiss, M. A., "Mixing and Distribution of Liquids in a High-Velocity Air Stream," *Industrial and Engineering Chemistry*, Vol. 45, No. 3, March 1953, pp. 667–677.

[14] Soo, S. L., *Fluid Dynamics of Multiphase Systems*, Blaisdell, Waltham, Mass., 1967, Chap. II.

[15] Edelman, R., "Turbulent Transport in Polydisperse Systems," TR 735, May 1970, General Applied Science Labs. Inc., Westbury, N. Y.

[16] Favre, A., "Statistical Equations of Turbulent Gases," *Problems of Hydrodynamics and Continuum Mechanics*, SIAM, 1969, pp. 231–266.

[17] Catton, I., Hill, D. E., and McRae, R. P., "Study of Liquid Jet Penetration in a Hypersonic Stream," *AIAA Journal*, Vol. 6, No. 11, Nov. 1968, pp. 2084–2089.

[18] Kolpin, M. A., Horn, K. P., and Reichenbach, R. E., "Study of Penetration of a Liquid Injectant Into a Supersonic Flow," *AIAA Journal*, Vol. 6, No. 5, May 1968, pp. 853–858.